CRYSTAL GROWTH & DESIGN
2007
VOL. 7, NO. 12
2778–2787

Structure and Stability of Triglyceride Monolayers on Water and Mica Surfaces

Aneliya N. Zdravkova and J. P. J. M. van der Eerden*

Department of Condensed Matter and Interfaces, Utrecht University, P.O. Box 80000, 3508 TA Utrecht, The Netherlands

Received October 12, 2006; Revised Manuscript Received June 19, 2007

ABSTRACT: The structure and the stability of tripalmitin (PPP), tristearin (SSS), and triarachidin (AAA) monolayers at the air−water interface are investigated with the Langmuir method. The Langmuir−Blodgett (LB) layers obtained by deposition on mica were investigated with atomic force microscopy (AFM). Our experiments show that the three triglycerides can form monolayers with molecules in trident conformation at the air−water interface. We determined the equilibrium spreading pressure π_{eq} below which such monolayers are thermodynamically stable. Under isobaric conditions, a slow compression was sometimes observed for PPP and SSS, corresponding to crystal formation with molecules in tuning fork conformation on top of the monolayer. This isobaric compression takes place at pressures significantly larger than π_{eq} but still smaller than the collapse pressure. The isobaric compression rate was highest for PPP and almost zero for AAA. Through the use of AFM, the thickness of the trident monolayers was measured. It is 1.49 for PPP, 1.75 for SSS, and 2.2 nm for AAA, corresponding to tilt angles of the molecules of about 46, 49, and 59°, respectively. The LB monolayers of PPP and SSS are thermodynamically unstable in air. Small crystals form on top of the monolayer, presumably in β-phase for SSS. Domains with α-like and β-like structure coexist in the LB film of PPP. The nucleation rate increases with increasing surface pressure π and with decreasing chain length of the triglyceride. For AAA, no well-defined crystals were found on top of the LB monolayer during the periods of days. The trident monolayer is the less mobile, and the crystal phase is the more stable the longer the alkyl chains are.

1. Introduction

The interfacial behavior of surfactants and their mixtures is of importance in a wide range of applications. The most commonly used emulsifiers in the food industry are the monoglycerides.[1] Spread monolayers at air−water interface can show relaxation phenomena mainly because of instability due to desorption or collapse.[2]

For monoglyceride monolayers, it was observed that the main causes of instability are the desorption in subphase competing with collapse followed by nuclei formation. It was found that the stability of the monolayers depends on the film structure, subphase composition, the temperature, the surface pressure,[3,4] and aqueous phase pH.[5] Some of the investigated monoglycerides were unstable at surface pressures π below the so-called collapse pressure π_{col}. The rate of monolayer molecular loss due to desorption increased with surface pressure. Molecular loss at the interface depended also on the hydrocarbon chain length. The longer monoglycerides were more stable than the shorter ones.[3,5]

The triglycerides are another class of molecules of great importance in the food industry. They are isolated from plant seeds or animal tissues and are processed into edible fat products of which they are the main constituents. The crystallization of triglycerides is a key step both during manufacturing fat products and fractionating fats and oils. In all cases, the crystallization behavior is very complex because of the intricate composition of fat blends and the tendency of triglycerides to crystallize in a variety of morphological forms. Depending on the crystallization procedure, especially the thermal treatment, they may crystallize in the α (hexagonal, less stable), β' (orthorhombic), or β (triclinic, most stable) form. Each of these polymorphs consist of layers in which the molecules can pack with their acyl chains ("legs") in one of two conformations; neither involves all three chains packing alongside each other. They can pack in a "chair" conformation where the acyl chain in the 2 position is alongside the chain on either the 1 or 3 positions. Alternatively, a "tuning fork" conformation can be adopted where the acyl chain in the 2 position is alone and the chains in the 1 and 3 positions pack alongside each other.[6,7]

The $C_nC_nC_n$-type (n = even) triglycerides have double chain length structure, and the most stable phase is β. They have asymmetric tuning fork conformation.[8] Because this is the type of triglycerides that we investigated in this work, in the next chapters we will use tuning fork conformation to describe their crystal structure.

On the other hand, in monolayers at a hydrophilic−hydrophobic interface triglyceride molecules adopt a trident conformation (all hydrocarbon chains pointing toward the same direction). In the trident conformation, the hydrophilic glycerol group is in contact with the water or the mica surface, and the hydrophobic chains point into the air or oil.[9−13]

In previous work, we investigated monolayers of tristearin (SSS, chain length 18 C atoms) floating on water in a Langmuir system and deposited on mica with AFM. The Langmuir experiments showed that adsorption isotherms obtained with commonly used compression rates do not correspond to thermodynamic equilibrium. Under isobaric conditions, a slow compression was found, corresponding to the formation of crystals on top of the monolayer. The atomic force microscopy (AFM) images revealed that SSS initially forms trident monolayers at air−water interface. These layers are thermodynamically stable only at surface pressure $\pi \leq 5$ mN/m. For $\pi \geq 10$ mN/m, the growth of crystals takes place with a tuning fork conformation of the SSS molecules on top of the trident monolayer. The crystals grow with time, mainly in lateral directions. The growth rate increases with surface pressure. A new model was developed to quantitatively describe the crystal growth process. A lateral growth rate of 2.3 nm/min and a

* Corresponding author. E-mail: j.p.j.m.vandereerden@phys.uu.nl. Fax: 31 30 253 2403.

10.1021/cg060701t CCC: $37.00
Published on Web 11/15/2007

vertical growth rate of 0.005 nm/min were calculated for individual crystals at $\pi = 10$ mN/m. The same growth process that was observed on the air−water interface was also observed in transferred monolayers at room temperature, though the growth was much slower.[14]

The aim of this paper is to understand the behavior of different triglycerides (tripalmitin, PPP, chain length 16 C atoms; tristearin, SSS; and triarachidin, AAA, chain length 20 C atoms) at the air−water interface (Langmuir film) and on solid surface like mica (Langmuir−Blodgett (LB) film) and to establish the relationship between their molecular structure and their monolayer stability. Two kinds of experiments have been done. First, we measured the π−A (spreading pressure π versus area per molecule A) diagram of Langmuir films. Starting with a Langmuir film at very small π where the film is in a low-density "gas" phase, we compressed the film at a constant rate to the desired pressure π (forced compression). To investigate whether the Langmuir film was in thermodynamic equilibrium at this pressure π, we sometimes left the film for some time t at pressure π (isobaric compression). In the second type of experiment, the Langmuir film was transferred to mica directly after forced compression ($t = 0$). We investigated LB films with AFM immediately and a few days after incubation in air at room temperature.

2. Materials and Methods

2.1 Chemicals. (a) Film material. In our experiments, we used saturated monoacid triglycerides (their three acyl chains are the same). Tripalmitin (1, 2, 3-propanetriyl trihexadecanoate, PPP, chain length 16 C atoms), tristearin (1, 2, 3-trioctadecanoylglycerol, SSS, chain length 18 C atoms), and triarachidin (trieicosonoin, AAA, chain length 20 C atoms) were purchased from Larodan (Sweden) with a stated purity of >99 mass%. Stock solutions of PPP, SSS, and AAA with concentration of 1 mM in distilled chloroform were prepared.

(b) Subphase. Distilled water was used as a subphase in our Langmuir system for all experiments. The resistivity of the water was 15 MOhm cm.

(c) Substrates. All monolayers were transferred onto freshly cleaved mica.

2.2. Langmuir Method. Compression isotherms were measured on a commercial, fully automated Langmuir−Blodgett trough (model 311D, Nima Technology Ltd., England). The instrument was equipped with a Teflon trough (283.0 cm^2) and one Delrin barrier. The spreading pressure π was measured with an accuracy of about 0.1 mN/m. The film material was initially spread on the water subphase, dropping 30 μL of 1 mM stock solution dissolved in chloroform, using a 100 μL Hamilton syringe. The conditions were chosen such that initially the average area A per molecule is $A \sim 110$ Å^2.We started (asymmetric) film compression 2 min after spreading. In our system, two modes of operation were available. First, the forced compression mode where the position of the barrier, and hence the trough length $l(t)$ ahead of the barrier, is given. Then the resulting spreading pressure $\pi(t)$ is registered. In this mode, we chose barrier velocities of the order of 1 cm/min, which according to the literature should be slow enough that the Langmuir film stays close to thermodynamic equilibrium.

Second, we used the isobaric compression mode where a constant spreading pressure π is applied, and the resulting trough length $l(t)$ is monitored. Obviously if the film is in equilibrium at the applied pressure, then $l(t)$ is constant. In practice, however, we often found the barrier to move with velocities of the order of 1 μm/s.

Note that for estimating the collapse pressure π_{col} we used a Langmuir−Blodgett homemade instrument.[14] With the Nima 311D LB trough, π_{col} was difficult to reach because of technical problems. On the other hand, because the Delrin barrier is known to drastically improve the quality and reproducibility of the experiment, we used the Nima trough for all other data presented in this paper.[15]

2.3. LB Film Transfer. To obtain LB films, first a substrate was immersed perpendicularly in the aqueous subphase. We started with a very small initial surface pressure ($\pi = 0$ mN/m) and compressed the monolayer slowly (1 cm/min) to the final pressure. To obtain a LB film that is characteristic for forced compression, the film was transferred immediately by vertical pulling of the substrate through the air−water interface at a speed of 2 mm/min. During the transfer, the surface pressure was kept constant by appropriately moving the barrier. The transfer process takes a few minutes. After deposition, the LB films were dried in air and were kept in close containers until use. All experiments were done at 20 ± 1 °C.

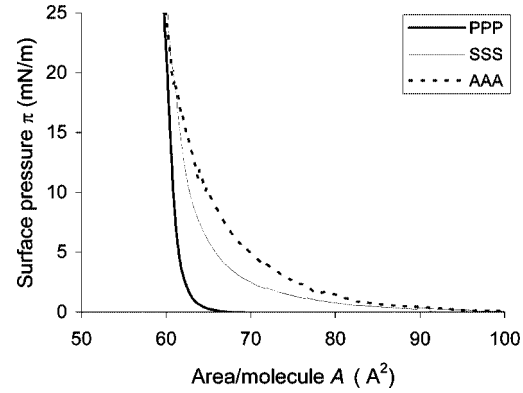

Figure 1. Surface pressure vs area isotherms of PPP, SSS, and AAA at the air−water interface at 20 °C, obtained by forced compression at a rate of 1 cm/min (thermodynamic equilibrium isotherms are obtained, in principle, at very slow compression rates).

2.4. AFM Measurements. The samples were examined with AFM immediately after preparation. Imaging was done with a Nanoscope (R) IIIa (Digital Instruments, Santa Barbara, CA) in contact mode with oxide-sharpened silicon nitride tip ($k = 0.06$ N/m). The AFM was equipped with a J-scanner (176 × 176 μm^2; z-limit = 5.349 μm). All images were processed using procedures for flattening in Nanoscope III software version 5.12r5 without any filtering. To check if the monolayer is successfully transferred to the mica surface we measured at least five different spots (each 150 μm^2) of every sample. To detect structural changes in the adsorbed film in contact with air, we studied LB films several days after incubation at room temperature (20 ± 1 °C) as well.

3. Langmuir Observations

3.1. Forced Compression. Figure 1shows typical π−A isotherms of PPP, SSS, and AAA, recorded at a barrier velocity of 1 cm/min. Two different regimes can be recognized for the three triglycerides. At a large area per molecule, A, the pressure is low and increases slowly with decreasing A. Below a certain value of A, the pressure increases more rapidly. We define the pressure and area where the change over between these regimes takes place as π_{cond} and A_{cond}. For convenience, we call π_{cond} condensation pressure and A_{cond} condensation area. For further interpretation of these values, see Section 3.3, especially Figure 4. We interpret the low-pressure regime as "gaseous" and the high-pressure phase as "condensed". On the basis of Langmuir experiments alone, we cannot conclude whether the condensed phase is liquidlike or solidlike. For $\pi \geq \pi_{cond}$, the molecules are close enough together to form a condensed monolayer. The collapse pressure π_{col} is the surface pressure at which the monolayer collapses to form multilayer structures. For the studied triglycerides, it was in the range of $\pi_{col} = 40$–48 mN/m and $\pi_{col}(AAA) < \pi_{col}(SSS) < \pi_{col}(PPP)$.

The measured π−A data showed that the transition from one regime to another was not very sharp, and it was different for the investigated triglycerides. To get reliable and unbiased estimations for A_{cond} and π_{cond}, we fitted the isotherms to

$$\pi(A) \approx \frac{2\pi_{cond}}{a} h(A - A_{cond}, a) \quad (1)$$

where A_{cond}, a, and π_{cond} are fitting parameters. The function

$$h(x, a) \equiv \frac{1}{2}(\sqrt{x^2 + a^2} - x) \quad (2)$$

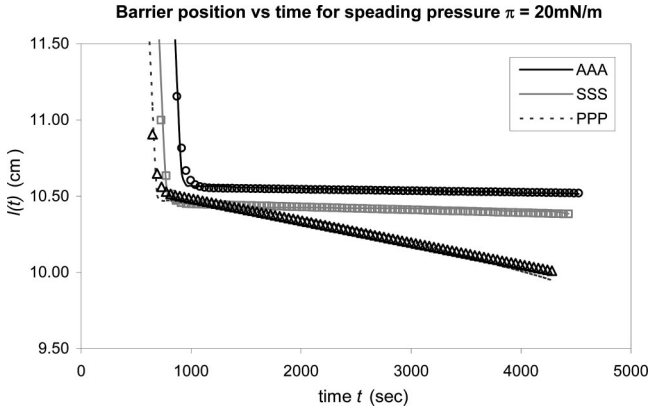

Figure 2. Examples of the measured barrier position as a function of time during forced and isobaric compression for (Δ) PPP, (□) SSS, and (○) AAA. The almost vertical parts of the curves correspond to forced compression rate of $\nu_f \approx 1$ cm/min. The slowly decreasing parts correspond to isobaric compression at velocity ν at the spreading pressure $\pi = 20$ mN/m. Note that the molecular loss, presented by $l(t)$ is higher for PPP.

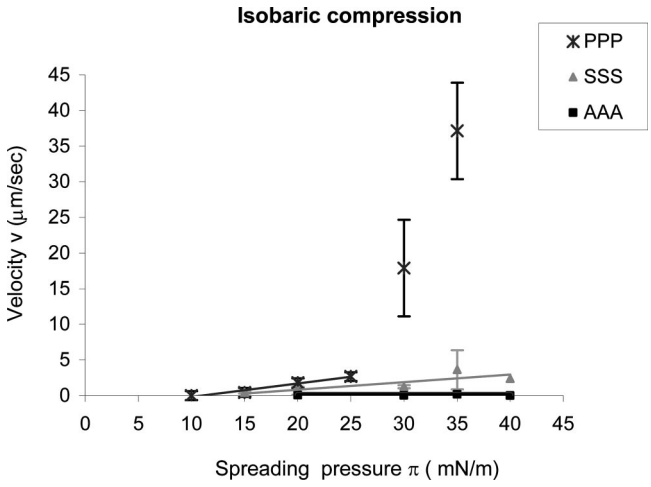

Figure 3. Isobaric velocity ν (μm/s) as a function of the spreading pressure π, as obtained by fitting the measured barrier position to eq 3 for PPP, SSS, and AAA. Note the sharp increase in ν for spreading pressure for $\pi \geq 30$ mN/m well below the collapse pressure $\pi_{col} \approx 48$ mN/m for PPP.

is a hyperbola interpolating between the asymptotes $h(x,a) \approx |x|$ for large negative x and $h(x, a) >> 0$ for large positive x. The asymptotes intersect at $h = a/2$ for $x = 0$. This function provides a convenient method to arrive at an unbiased estimation of π_{cond} and A_{cond}. From a number of isotherms that were obtained at compression velocity 1 cm/min, we found $A_{cond} = 62 \pm 1$ Å^2 and $\pi_{cond} = 6 \pm 2$ mN/m for PPP; $A_{cond} = 62 \pm 1$ Å^2 and $\pi_{cond} = 9 \pm 2$ mN/m for SSS; and $A_{cond} = 65 \pm 1$ Å^2 and $\pi_{cond} = 8 \pm 1$ mN/m for AAA.

The fact that A_{cond} is around 63 Å^2 for all studied triglycerides is consistent with a trident conformation of triglyceride molecules in a monolayer film at the air—water interface. Indeed, the cross-sectional area per hydrocarbon chain for tristearin at 20 °C in the α-phase (the α-phase has the most mobile acyl chains) is 19.7 Å^2.[16] Our isotherms are consistent with earlier reports.[9,13,14]

The fact that π_{cond} is almost the same for the investigated triglycerides as well, is consistent with the idea that the packing properties of the hydrocarbon chains are mainly determined by

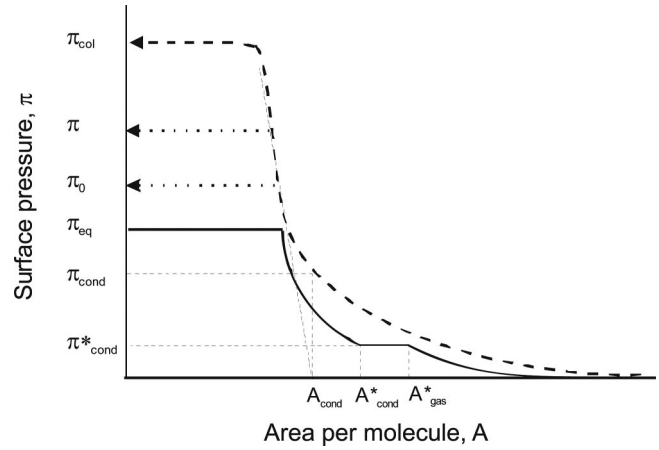

Figure 4. Schematic $\pi-A$ isotherm. The thick line is the reversible thermodynamic isotherm, which cannot be measured directly as it requires a compression rate of 0. π_{eq} and π^*_{cond} are the equilibrium pressures for monolayer-crystal and condensed-gaseous monolayer coexistence. The dashed line is a dynamic isotherm, and π_{cond} and A_{cond} are defined according to eq 1. The dotted arrows indicate isobaric compression. Although isobaric compression takes place in the whole range $\pi_{eq} < \pi < \pi_{col}$, for $\pi < \pi_0$ it is too slow to be experimentally measured.

short-range repulsive interactions. The effective repulsion is quite independent of the chain length.

The fitting parameter a describes the sharpness of the gas-condensed transition. Its value depends strongly on the chain length. We found a(PPP) $= 2 \pm 1$, a(SSS) $= 3 \pm 1$, and a(AAA) $= 6 \pm 2$. This is also seen in Figure 1, where the $\pi-A$ isotherm for PPP is sharper than those for SSS and AAA. This effect is partly of a kinetic nature, that is, PPP realizes the transition from gas to condensed phase faster than the longer SSS and AAA. Longer chains need more time to transform and rearrange in perpendicular position; correspondingly, we have a(PPP) $<$ a(SSS) $<$ a(AAA). However, if this difference in sharpness was solely due to the mobility of individual triglycerides, the value of a would strongly depend on the compression rate. As we did not observe such dependence,[14] we conclude that the sharpness of the triglycerides isotherms is partly determined by the interactions between the molecules. From this perspective, we shall discuss the experimental results in the next section.

3.2. Isobaric Compression. To investigate the stability of the triglyceride films at an air−water interface, we made the following experiment. We stopped the forced compression at a constant compression rate ν_f when a certain surface pressure π was reached. Next, we kept the surface pressure constant at that value, allowing the barrier to move. After several minutes, a constant isobaric velocity ν was reached usually. Because of molecular loss from the monolayer, the barrier moved forward to keep the surface pressure constant and the through length $l(t)$ decreased. This is shown in Figure 2.

The evolution of the trough length was fitted to

$$l(t) \approx l_0 - v(t - t_0) - (v_f - v)h(t - t_0, a) \qquad (3)$$

Here, the five fitting parameters are l_0, the trough length at the start of the isobaric compression; t_0, the starting time of the isobaric period; ν_f and ν, the forced and isobaric barrier velocity, respectively; and a, characterizing the transition from the forced to the isobaric regime. The accuracy of the fits typically was 0.2%. In all cases, the fitted forced velocity ν_f was very close to the applied barrier velocity.

3.3. Equilibrium versus Dynamic Adsorption Isotherms. In previous work,[14] we found that for SSS the adsorption isotherms that were obtained by forced compression did not change appreciably when increasing the barrier velocities from 0.5 to 2 cm/min. Nevertheless, under isobaric conditions we observed further compression. Isobaric velocities were 1 or 2 orders of magnitude smaller than common forced velocities. We observe the same behavior here for PPP and AAA. In Figure 3, we show the dependence of the isobaric velocity ν on the surface pressure π for the three triglycerides. At very small π, no compression rate could be detected ($\nu \approx 0$). At intermediate pressures, we observe isobaric compression ($\nu > 0$). In the case of PPP, the isobaric compression rate increases sharply for $\pi \geq 30$ mN/m, that is, well below the collapse pressure. These results show that the isotherms in Figure 1 should be considered as dynamic, rather than equilibrium isotherms for $\pi > 10$ mN/m. For such pressures, the equilibrium spreading pressure at a given value of A is smaller than the dynamic value given in Figure 1 (see Figure 4).

It is important to clearly discriminate between thermodynamic and dynamic isotherms. The former corresponds to thermodynamic equilibrium and should be obtained from a reversible compression. The difference is explained in Figure 4. Three different phases are included: a gaseous phase, a condensed monolayer (liquid or solid like), and a three-dimensional (3D) crystal phase. The coexistence gap $A^*_{gas}-A^*_{cond}$ between gaseous and condensed monolayer may be small or even absent.

For pressures $\pi > \pi_{eq}$, the monolayer is unstable and tends to transform to a crystalline phase.[17] During isobaric compression, the film effectively thickens. Using AFM, we have shown that this is due to growth of 3D crystals on top of the monolayer, which is what one should expect for $\pi > \pi_{eq}$. For $\pi > \pi_{col}$, the same crystallization process takes place but in a less controlled and less reproducible manner. Note that sometimes one calls equilibrium-spreading pressure what we would call collapse pressure (see, e.g., ref 5). For $\pi = \pi_{eq}$, the chemical potentials μ_β of triglycerides in the β-phase and μ_L of triglycerides in the Langmuir layer on the water surface are equal.

$$\mu_L(\pi = \pi_{eq}) \equiv \mu_\beta$$

In principle, we can estimate π_{eq} from the dependence of the isobaric velocity ν on π ($\nu(\pi \leq \pi_{eq}) = 0$). In Figure 3, we see that there exists a surface pressure π_0, such that $\nu \approx 0$ for $\pi \leq \pi_0$. Naively, we might assume that $\pi_0 \approx \pi_{eq}$. On the other hand, we know from our AFM observation that the process taking place for $\pi > \pi_0$ is crystal growth. In general, a nonlinear dependence of the crystal growth rate on π is expected. For example, for faceted crystals a so-called "nucleation gap" is known to exist, meaning that for π in the regime $\pi_{eq} \leq \pi \leq \pi_0$, no observable growth takes place. Thus, the equilibrium pressure π_{eq} may be well below π_0. According to Figure 3 for PPP at the air−water interface, $\pi_0 = 10$ mN/m. The compression rate for PPP at $\pi > \pi_0$ increases with increasing surface pressure, as does the monopalmitin monolayer on water.[3,5] The isobaric velocity for SSS given here is slightly smaller than measured before,[14] and $\pi_0 = 15$ mN/m is higher (Figure 3). From our experiments, it was difficult to estimate π_0 for AAA. The measured isobaric velocity was too small over the whole range of investigated surface pressures (Figure 3).

From our experiments, it can be concluded that both the mobility, characterized by ν, and the effective stability, characterized by π_0, of triglyceride monolayers at an air−water interface depend on the film material, notably on the length of the triglycerides. The observation ν(PPP) > ν(SSS) > ν(AAA) in Figure 3 can be understood as the mobility and flexibility will decrease with increasing chain length.

The increasing interaction strength will also influence the thermodynamic stability of the crystal phase, for example, an increasing melting point and a decreasing equilibrium vapor pressure. Therefore, one would expect π_{eq}(PPP) ≥ π_{eq}(SSS) ≥ π_{eq}(AAA). This seems contradictory to π_0(PPP) < π_0(SSS) that we see in Figure 3. It is well-known, however, that a stronger molecular interaction generally leads to stronger nonlinearity of the dependence of the growth rate and the nucleation rate on $\pi-\pi_{eq}$. As a consequence, the nucleation gap $\pi_0-\pi_{eq}$ will be larger for SSS than for PPP. Only if we could make full nonlinear $\nu(\pi)$ fits to data like those in Figure 3, we might find the real dependence of π_{eq} on the chain length.

4. AFM Observations

4.1. Monolayer Thickness. In ref 14, we showed that SSS molecules form a trident monolayer at an air−water interface, which can be transferred to mica. We found that the monolayer thickness varied from 1.6 to 1.8 nm over the pressure range we studied. The molecules were tilted, and the tilt angle varied from $\tau = 43°$ at $\pi = 10$ mN/m to $\tau = 53°$ at $\pi = 40$ mN/m.

From the AFM images of LB films of PPP, SSS, and AAA withdrawn at $\pi = 20$ mN/m (Figure 5), it is seen that the mica substrate is covered by a homogeneous monolayer. Apparently, the Langmuir monolayer can be successfully transferred from the water surface in the Langmuir trough to a mica surface to form a LB film there. When the LB films were prepared at lower pressures (data not shown), a monolayer was observed as well but with a lot of holes in it.

We estimated the monolayer thicknesses d_0 using the following procedure. By scanning with a relatively large force, $F >> 30$ nN, we scratched a rectangular hole in the monolayer with the AFM tip. Then a larger area, including the hole, was scanned with small forces gradually increasing from $F = 1$ to $F = 8$ nN (Figure 5). The height difference between the hole and the surrounding film gives an apparent thickness d'. Analyzing our data carefully, we found that d' turned out to depend on the scanning force F for all investigated triglycerides. Therefore, the real monolayer thickness d_0 differs from d'. In Figure 6, we present the observed dependence of d' on F. It is seen that d' is larger for larger chain length, as expected. It is also seen that the vertical compression of the monolayer, given by the slope of $d'(F)$ curves, is the same for PPP, SSS, and AAA. The real thickness $d_0 = d'(F = 0)$, corresponding to zero-scanning force, is presented in Figure 7. It is linearly dependent on the length of the chains in the triglyceride molecules.

To translate the thickness into a tilt angle τ of the acyl chains with the mica surface, we need to estimate the effective chain length. A precise analysis and interpretation of crystallographic data for the long spacing $d(001)$ of PPP, SSS, and AAA in the stable β-phase[8] allows us to estimate an effective length d_{eff} of PPP, SSS, and AAA molecules in tuning fork conformation. Correcting this for the length of the glycerol group and the contribution from the contact region of (001) layers in the β-phase, the alkyl chain length d_{chain} can be estimated. When carrying out an analogous procedure for the α and β' phase, the same lengths d_{chain} are found.

We cannot deduce detailed information on the molecular conformation of the triglyceride molecules in the monolayer from our AFM experiment. To estimate the tilt angle in the monolayer, we assume that the glycerol part of the molecule makes close contact with the (hydrophilic) substrate and that the alkyl chains are stretched similar as in α, β, and β' phases,

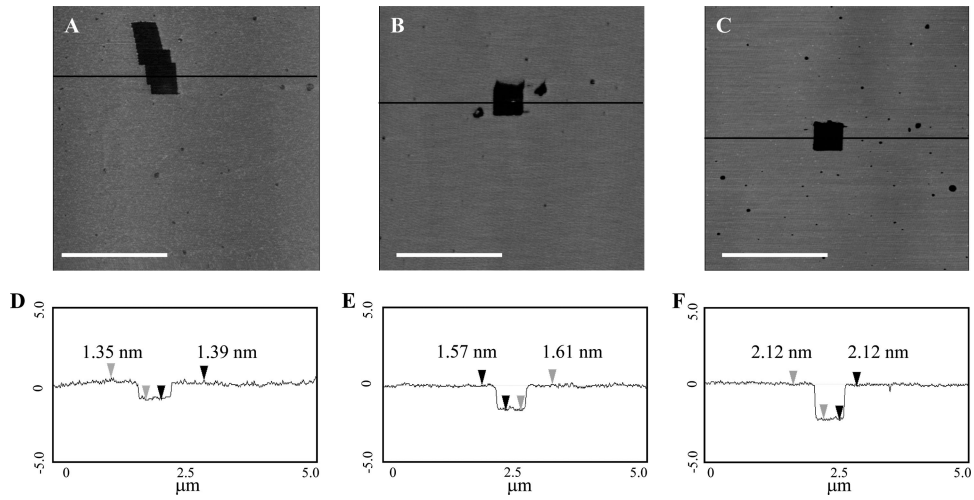

Figure 5. AFM height image of monolayers transferred immediately after forced compression to surface pressure $\pi = 20$ mN/m. The black squares are holes in the monolayer produced by scanning at a high AFM force ($F \sim 30$ nN). The monolayers are scanned at AFM force $F = 1$ nN. (A) PPP monolayer with corresponding cross-section (D). (B) SSS monolayer and the corresponding cross-section (E). (C, F) AAA monolayer. The scale bar is 2 μm, and the vertical scale is 10 nm for all images.

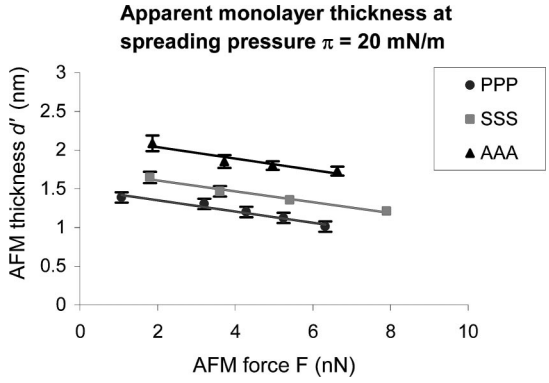

Figure 6. Measured layer thickness d' for PPP, SSS, and AAA as a function of applied AFM force F at surface pressure $\pi = 20$ mN/m.

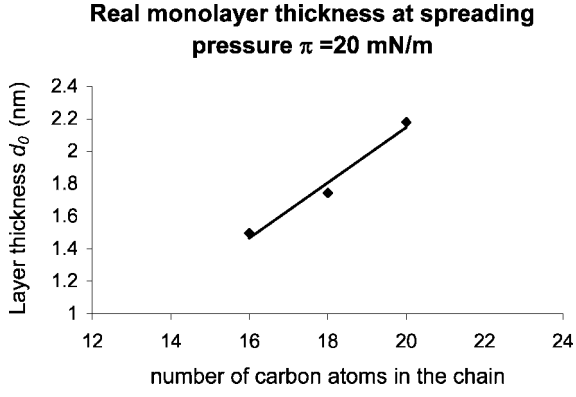

Figure 7. Real monolayer thickness d_0 for PPP (16), SSS (18) and AAA (20) at surface pressure $\pi = 20$ mN/m. The values are found by extrapolation of the apparent monolayer thickness d' in Figure 6 to AFM force $F = 0$ nN.

though in different orientation with respect to the glycerol group. This leads to a structure where alkyl chains d_{chain} extend from the substrate to the monolayer surface at a height d_0 above the substrate. Thus, in the monolayer the triglyceride molecules adopt a trident conformation to get the simple relation

$$\sin(\tau) = d_0/d_{chain} \quad (4)$$

Table 1

triglyceride	$d(001)$ β-phase (nm)	d_{eff} (nm)	d_{chain} (nm)	d_0 (nm) of monolayer	tilt angle τ
PPP	4.03	4.62	1.80	1.49	46.4
SSS	4.48	5.13	2.31	1.75	49.2
AAA	4.92	5.62	2.82	2.20	59.0

The estimated chain lengths and the lower limit of the tilt angles are given in Table 1. Another explanation for the measured smaller thickness of the monolayer could be that the three alkyl chains cannot all have an all-trans configuration. In this case, the defects will be retained in the deposited layer, giving a resultant layer with a thickness less than the all-trans length. In view of this, the estimated tilt angle in the table should be considered as a lower limit. The calculated d_0, however, is so much less than d_{chain} that significant tilt ($\tau < 90°$) is likely. Moreover, for SSS,[14] we found that the monolayer thickness increases with increasing surface pressure. This can be explained with an increase of the tilt angle τ due to compression. Such an increase in the tilt angle upon compressing a monolayer of long chain molecules (fatty alcohols and acids) was calculated on the basis of X-ray measurements.[18–20]

In the stable β-phase, the triglyceride molecules are tilted at tilt angle $\tau = 60.8°$.[8] Because presumably in the trident monolayer the alkyl chains are less densely packed than the crystalline phases, a smaller tilt angle seems acceptable. Interpreting our monolayer thickness data with eq 4, we see that the tilt angle increases with increasing the length of the alkyl chains, that is, the longer chains in the monolayer are more perpendicular to the substrate than the shorter chains. In the aliphatic alcohol monolayers on water, the same dependence of the tilt angle on the chain length was found. IR spectra of these alcohol monolayers showed that the hydrocarbon chains become more ordered with increasing length.[21]

4.2. Stability of the Transferred LB Film. In our previous investigations, we found that during incubation in air, the transferred SSS films become slightly thicker and grainy. Crystals that were present directly after the transfer were growing, and new, very small nuclei appeared.[14] We suggested that the grainy character of the monolayer is due to small clusters of molecules, which leave the monolayer to form new crystals or contribute to the growth of existing crystals. The crystal-

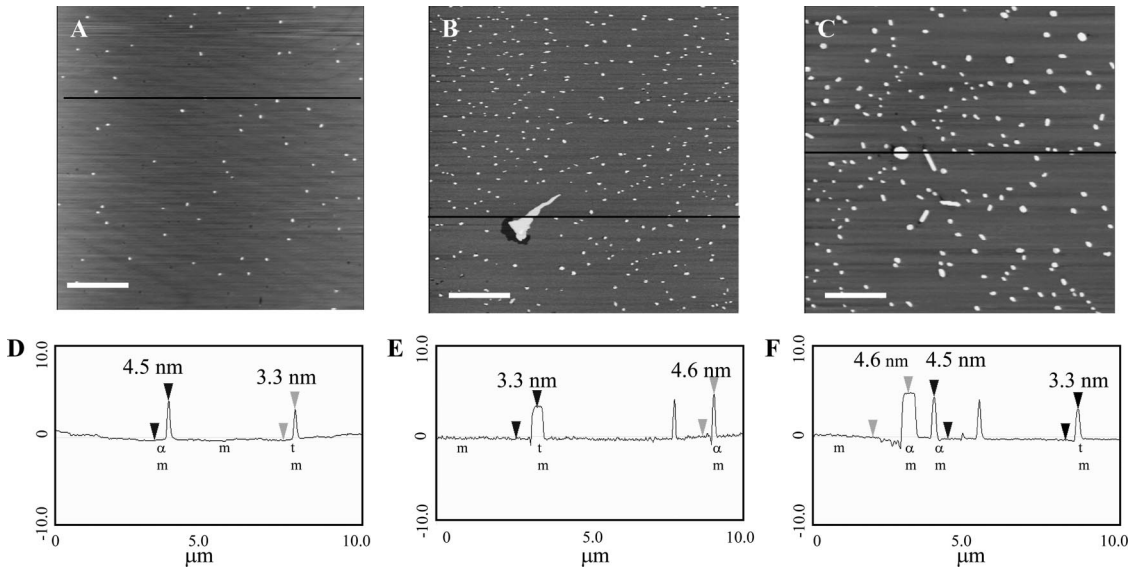

Figure 8. AFM height image of PPP monolayers transferred at $\pi = 20$ mN/m: (A) immediately after forced compression, (B) the same sample after 1 day incubation in air at room temperature, and (C) the same sample after 2 days incubation in air. The corresponding cross-sections are given in D−F. The scale bar is 2 μm, and the vertical scale is 20 nm for all images. Height differences are given by the numbers at the markers. The symbols below the lines give our proposed structure of the crystals (m, monolayer in trident conformation; t, top layer in tuning fork conformation; α, crystal in tuning fork conformation).

lization is caused by the energetically unfavorable trident conformation of the molecules, as compared to the tuning fork conformation. To investigate this mechanism further, we transferred PPP, SSS, and AAA Langmuir layers to mica, immediately after forced compression to spreading pressure π and left them in closed containers for a few days at room temperature (20 ± 1 °C).

(a) Initial Structure and Structural Changes of PPP monolayer. After a 30 min incubation on the water surface at surface pressure $\pi = 10$ mN/m (this is π_0 for PPP), which we expect to be close to π_{eq} for PPP, the AFM images show a homogeneous monolayer with small holes when the LB film was transferred to mica (data not shown). At surface pressure $\pi = 20$ mN/m, which is well above π_0, we found that the directly transferred PPP film consists of a condensed monolayer onto which many small domains were positioned. The thickness of the domains ranged from 3.3 to 4.6 nm above the monolayer level (panels A and D in Figure 8). On the basis of the estimated effective length of 4.62 nm for a PPP molecule in tuning fork conformation, the observed domain thickness of 3.3 ± 0.1 nm corresponds to a tilt angle $\tau = 43.8$–$47.3°$, which is between the estimated tilt angle in the trident monolayer and the tilt angle in the stable β-phase ("t" in the figures). The height of 4.5 ± 0.1 nm corresponds to fully extended PPP molecules (4.62 nm) that are almost perpendicular to the substrate, similar to the crystalline α-phase. Judging from the thickness of the domains, most of them were in the α-phase, and some were in the β-phase. These domains were soft and could be easily scratched away with the AFM tip, even at the low AFM forces that are normally used for imaging. Indeed, after a few scans with $F =$ 1–2 nN, these domains usually disappeared, leaving a flat film with the thickness of the trident monolayer. This result is consistent with the growth of crystals in tuning fork conformation on top of the trident monolayer, reported for SSS.[14] We therefore may assume that the observed domains are small crystals, formed in the period where the spreading pressure increased from the small values at which the film is in a two-dimensional gas state to the final pressure $\pi-\pi_0$ at which the condensed phase has formed. In this period, PPP molecules

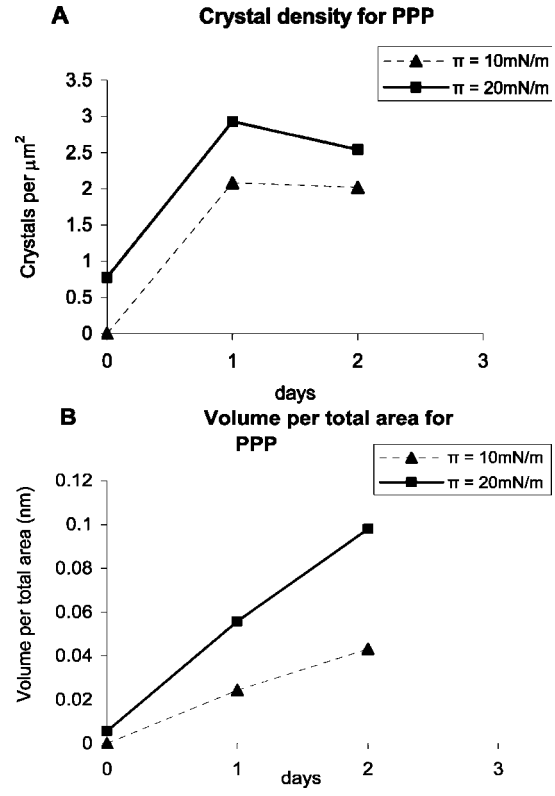

Figure 9. Crystals per area (A) and volume per total area (B) formed during incubation of PPP LB monolayer in air at room temperature.

undergo major orientation and packing changes. As a result, the formation process of the domains will not be strictly deterministic, and a metastable film structure may form. The domains serve as crystal seeds that can grow into bigger crystals when the LB film is incubated a longer time in air (Figure 8).

The AFM images of LB films of PPP incubated for 1 day in air showed that the monolayer is still present and the density of the crystals is higher. Most of the new crystals were small

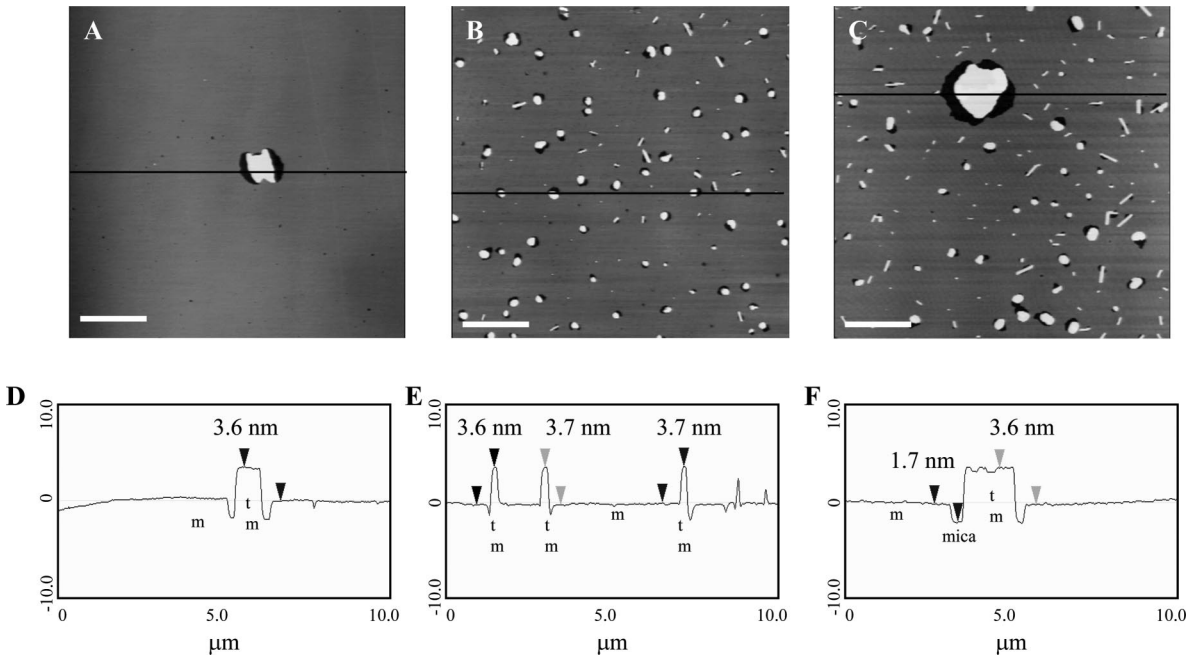

Figure 10. AFM height image of SSS monolayers transferred at $\pi = 20$ mN/m: (A) immediately after forced compression, (B) the same sample after 1 day incubation in air at room temperature, and (C) the same sample after 2 days incubation in air. The corresponding cross-sections are given in D−F. The scale bar is 2 μm, and the vertical scale is 20 nm for all images. Height differences are given by the numbers at the markers. The symbols below the lines give our proposed structure of the crystals (m, monolayer in trident conformation; t, top layer in tuning fork conformation).

and with a thickness of 4.6 ± 0.1 nm. Some bigger domains were found with a thickness of 3.3 ± 0.1 nm (panels B and E in Figure 8). After 2 days incubation, the domains were bigger, mostly with a thickness of 4.6 ± 0.1 nm and still surrounded by the trident monolayer (panels C and F in Figure 8). The dark regions around the crystals are holes in the monolayer. The original monolayer material has accumulated in the crystals that have grown. Apparently immediately after the transfer, a few crystals are present; some are in α-phase and others are in β-phase. In air, these crystals grow, and new crystals, mostly in α-phase, nucleate. The same processes were observed for PPP monolayer transferred at $\pi_0 = 10$ mN/m after a few days incubation in air, but the speed of nucleation is lower (Figure 9).

From these observations, we conclude that the LB monolayer is unstable both with respect to the α-phase and to the β-phase, as shown in the following equation:

$$\mu_{LB}(\text{PPP}) > \mu_{\alpha}(\text{PPP}) > \mu_{\beta}(\text{PPP}) \quad (5)$$

where μ_{LB}(PPP) is the chemical potential of PPP molecules in a monolayer on the mica surface. Note that from the LB layer, the less stable α-phase mainly grows. This is a manifestation of Ostwalds rule, which states that if two (or more) phases can grow in principle, then the least stable of these phases usually will dominate because it is less ordered, and hence its growth kinetics are faster.

(b) Initial Structure and Structural Changes of SSS Monolayer. When the SSS film was withdrawn after 30 min incubation at the air−water interface at $\pi = 15$ mN/m (this is π_0 for SSS), we observed only a homogeneous (trident) monolayer with a lot of holes. After 2 days incubation in air, the LB monolayer was covered with small domains with a thickness of 3.6 ± 0.1 nm (data not shown). At surface pressure $\pi = 20$ mN/m ($\pi > \pi_0$), we found that the directly transferred SSS film consisted of an almost defect free monolayer in which a few domains were imbedded. The thickness of the domains was 3.6 ± 0.1 nm (panels A and D in Figure 10). After 1 day incubation in air, the LB monolayer was covered with many new nuclei with a thickness of 3.6 ± 0.1 nm (panels B and E in Figure 10). After 2 days incubation in air, the observed nuclei were bigger and all with the same thickness (panels C and F in Figure 10). The observed domain thickness of 3.6 ± 0.1 nm corresponds to a tilt angle of $\tau = 43$–$44.5°$, that is, somewhere between the estimated tilt angle in the trident monolayer and the tilt angle in the stable β-phase. We suppose that the structure of these layers can be described as a slightly deformed β or β' phase. As we observed that this layer thickness was always at the upper crystal layer, as was also for multilayer crystals, we referred to this structure as the top layer structure (t in the figures).

The structure of SSS films immediately transferred after forced compression to $\pi = 30$ mN/m was reported in our previous work.[14] Most of the observed crystals had a thickness of 4.9 ± 0.1 nm above the monolayer level. This thickness corresponds to fully extended alkyl chains of SSS (panels A and D in Figure 11). When the LB monolayer was incubated in air for 1 day, the existing crystals grew, and new, very small nuclei appeared. The thickness of the new nuclei and the newly grown parts of the crystals was 3.6 ± 0.1nm (panels B and E in Figure 11). After 2 days incubation in air, the new nuclei became bigger (panels C and F in Figure 11).

The density of the crystals of SSS formed during incubation in air was initially growing with time (Figure 12A). Note, however, that the density at $\pi = 30$ mN/m after 2 days of incubation did not increase very much. This was due to coalescence of the large number of relatively large crystals at this pressure. The volume per total area of the crystals increased with the surface pressure and the time during the incubation (Figure 12B).

Summarizing, we found that for SSS immediately after transfer, several crystals were observed, which were mainly in

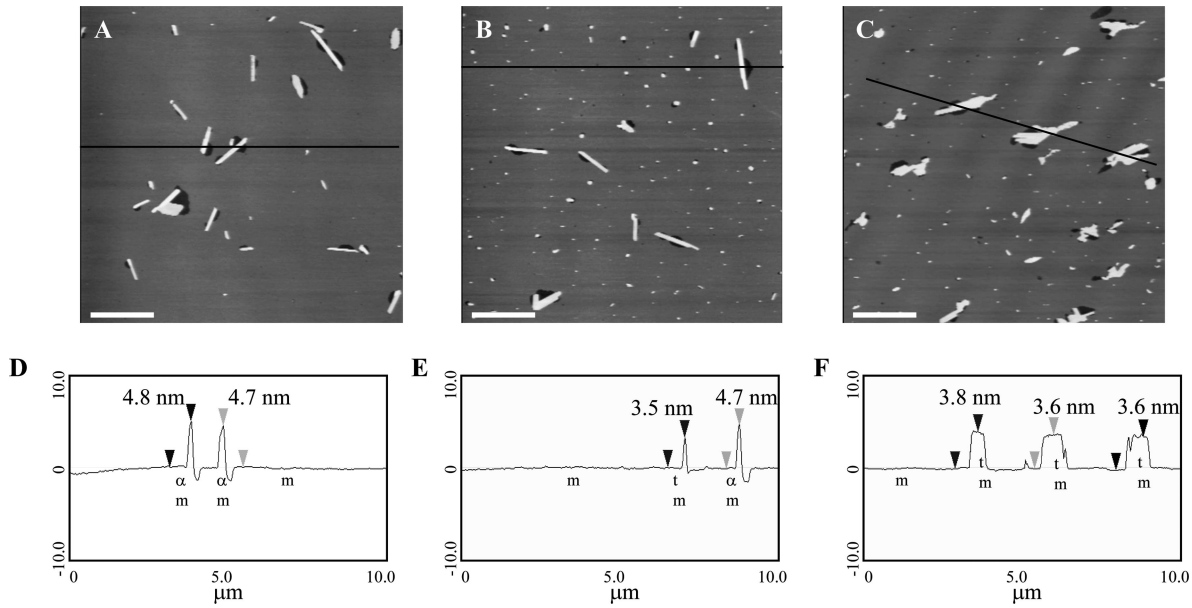

Figure 11. AFM height image of SSS monolayers transferred at $\pi = 30$ mN/m: (A) immediately after forced compression, (B) the same sample after 1 day incubation in air at room temperature, and (C) the same sample after 2 days incubation in air. The corresponding cross sections are given in D−F. The scale bar is 2 μm, and the vertical scale is 20 nm for all images. Height differences are given by the numbers at the markers. The symbols below the lines give our proposed structure of the crystals (m, monolayer in trident conformation; α, crystal in tuning fork conformation; *t*, top layer in tuning fork conformation).

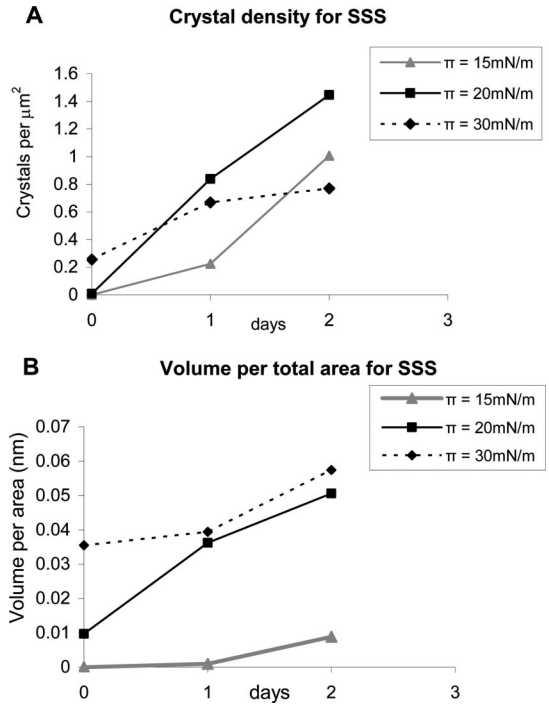

Figure 12. Crystals per area (A) and volume per total area (B) formed during incubation of SSS LB monolayer in air at room temperature.

the β-phase for $\pi \leq 20$ mN/m and mainly in the α-phase for $\pi \geq 30$ mN/m. This suggests that π_0(SSS, β) is 15mN/m or smaller, and π_0(SSS, α) ∼ 25 mN/m. The fact that $\pi_0(\alpha) > \pi_0(\beta)$ can been explained is because $\pi_{eq}(\alpha) > \pi_{eq}(\beta)$, the β-phase is more stable than the α-phase, and the nucleation gap $\pi_0 - \pi_{eq}$ probably is not much different for α and β. After transfer to mica surface, the existing crystals grow further and new crystals appear all mainly in the β-phase but not with respect to the α-phase. In terms of chemical potentials, this means that

$$\mu_\alpha(\mathrm{SSS}) > \mu_{LB}(\mathrm{SSS}) > \mu_\beta(\mathrm{SSS}) \quad (6)$$

Note that the location of the LB chemical potential with respect to μ_α and μ_β is different for SSS and for PPP.

(c) Initial Structure and Structural Changes of AAA Monolayer. When a LB film of AAA was transferred immediately after forced compression at $\pi = 20$ mN/m and incubated 2 days in air, we did not observe any crystals, but the monolayer was somewhat coarse. We suppose that this coarsening was due to very small nuclei, which were difficult to detect directly with the AFM. If we would have incubated the monolayer for a longer time, then probably the existing nuclei would grow into crystals. The absence of well-developed crystals after 2 days incubation is due to very slow kinetics of AAA. In terms of chemical potentials, we hypothesize the same relative positions as for SSS The slower kinetics of the AAA monolayer (as compared to SSS and PPP) is expected in view of the stronger interaction between the longer alkyl chains of AAA.

5. Discussion

By definition trident monolayers formed of PPP, SSS, and AAA are thermodynamically stable for $\pi \leq \pi_{eq}$ at the air−water interface. We discussed several methods to estimate π_{eq}. First, from the collapse pressure π_{col}. This leads to a large overestimation, $\pi_{col} \gg \pi_{eq}$. A practical estimate is π_{cond}, obtained from fitting experimental isotherms. We found $\pi_{cond} \sim 8$mN/m for all three triglycerides. The reliability of the assumption $\pi_{cond} \approx \pi_{eq}$, however, is unclear both theoretically and experimentally as π_{cond} may depend on the forced compression rate and π_{eq} does not. From isobaric compression, we estimate a pressure π_0 below which compression is absent or too slow to be measured. It is clear that $\pi_0 \geq \pi_{eq}$, but unfortunately the amount of overestimation, that is, the nucleation gap $\pi_0 - \pi_{eq}$, cannot

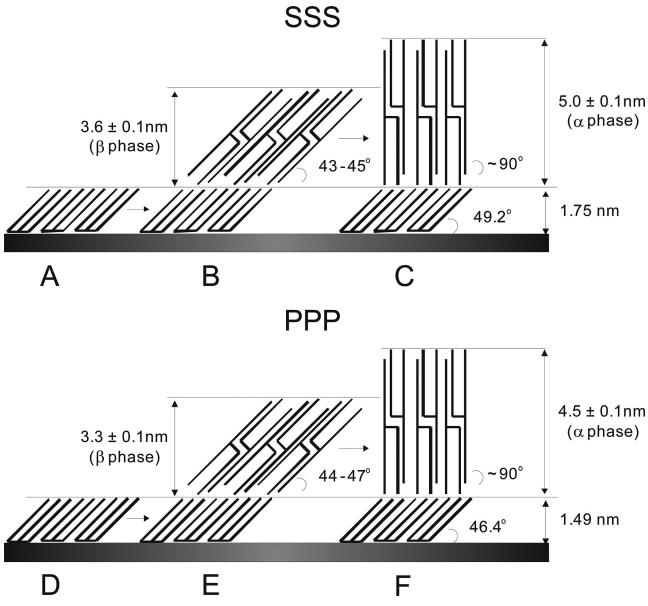

Figure 13. Schematic illustration of possible structures proposed for thin layers of SSS (A−C) and PPP (D−F).

be deduced from our data. We did not observe any changes in the structure of the trident monolayers on the air−water interface in the regime $\pi \leq \pi_0$. Combining all our observations with a physically reasonable picture, we conclude that $\pi_{eq} \leq 10$ mN/m for all three triglycerides, thus supporting the idea $\pi_{eq} \approx \pi_{cond}$. For all $\pi > \pi_{eq}$, the Langmuir monolayers are thermodynamically unstable though this becomes evident in the compression data only for $\pi > \pi_0$ and in the dynamic isotherms only for $\pi > \pi_{col}$.

Under isobaric conditions, slow compression rates were found for PPP and SSS. The isobaric velocity was highest for PPP and was almost zero for AAA. We demonstrated that the stability and the kinetics of Langmuir monolayer depend

$$\mu_{\alpha}(AAA) > \mu_{LB}(AAA) > \mu_{\beta}(AAA) \tag{7}$$

strongly on the length of the triglycerides alkyl chains. The longer the alkyl chains are, the less mobile the trident monolayer is and the more stable the crystal phase is.

The AFM images of LB films transferred immediately after forced compression at $\pi > \pi_0$ for PPP and SSS showed some domains on top of the monolayer. The molecules in these domains presumably adopt the tuning fork conformation and pack similar as in the crystalline α- and β-crystal forms (Figure 13).

Even though the compression rate for SSS trident monolayer at $\pi_0 = 15$ mN/m was $\nu = 0$, the LB monolayer that was transferred changed its structure during incubation in air. Small nuclei were formed with a thickness of 3.6 ± 0.1 nm, which corresponds to the β- or β'-phase (Figure 13B). The same crystal growth process takes place during incubation in air of the LB monolayer of SSS that was transferred at $\pi \geq 20$ mN/m (Figures 10 and 11). The density of the nuclei increased with the time (Figure 12A). On a LB film of SSS transferred at surface pressure $\pi = 30$ mN/m initially, some α-like structures (Figure 13C) were found, but they did not grow over time. The newly formed parts around them, and all new nuclei as well, were in β- or β'-phase (Figure 13B). Domains that were grown in the metastable, α-like, polymorph phase on the water surface do not spontaneously transform to the β- or β'-phase because this would involve a very slow solid−solid transformation process. We conclude that on mica, β is more stable than a trident monolayer, and α is probably not. Stated in terms of chemical potentials, this is expressed in eq 6 in Section 4.2b.

PPP behaves similar to SSS. The Langmuir monolayer of PPP does not change at the air−water interface at $\pi \leq 10$ mN/m, and it is thermodynamically unstable at $\pi > 10$ mN/m. Domains with a different thickness were found in the LB monolayer that was transferred immediately after forced compression at $\pi = 20$ mN/m (panels A and D in Figure 8). Apparently, domains with an α-like and a β-like structure coexist in the LB film of PPP (panels E and F in Figure 13). All transferred LB monolayers at $\pi \geq 10$ mN/m change during incubation in air. The AFM images showed that after incubation in air, small nuclei in the α-phase and β-phase appeared on top of the PPP monolayer, and their density increased extremely over time (Figure 9A).

Comparing Figures 9 and 12, we see that the growth and nucleation rates depend on the surface pressure and the nature of the triglyceride. The LB monolayers, which were transferred at $\pi \geq \pi_{eq}$, are thermodynamically unstable in air. The different mobility of the molecules in the trident monolayer of SSS and PPP is the main reason for the different rate of nucleation. The increase of the nucleation rate with increasing π reflects that the initial monolayer on mica is denser, and hence more unstable, when the Langmuir layer is transferred at higher π. Indeed, we may expect that the chemical potential of monolayer on mica is close to the chemical potential of the monolayer on water, that is, $\mu_{LB}(t = 0) \approx \mu_L(\pi)$. The monolayer molecules thus can reduce their free energy from about $\mu_L(\pi)$ to μ_α or μ_β by moving to the top of the monolayer to form new crystals in tuning fork conformation.

On the basis of our results for isobaric velocity at the air−water interface (Section 3.2), we concluded that PPP has a smaller π_0 (corresponding to faster kinetics) than SSS, even though π_{eq} is larger. The same will be true for layers on mica. For PPP, both the α- and β-phase are more stable than the LB monolayer. The driving force for β-formation is larger than for α-formation, but the kinetics are faster for α; therefore, we observe both domains with α-like and β-like structure. For SSS only the β-phase seems more stable. Also, for the longest triglyceride AAA, the monolayer is thermodynamically unstable at the air−mica interface, but the crystallization kinetics are so slow that on the time scale of days or even weeks, they behave as if they were stable.

6.Conclusions

In this study, we investigated the behavior of three triglycerides: PPP, SSS, and AAA at the air−—water interface and on a solid substrate. On the basis of Langmuir and AFM experiments, we established the relationship between the molecular structure and the stability of the monolayers. Our investigations led to the following conclusions.

At the air−water interface, all investigated triglycerides form monolayers of molecules in trident conformation. These monolayers are kinetically stable at the air−water interface at surface pressure $\pi \leq \pi_0$. π_0 is the surface pressure below which we did not observe any changes in the Langmuir monolayer under isobaric conditions. We know that $\pi_0 \geq \pi_{eq}$, where π_{eq} is the thermodynamic equilibrium pressure, but the amount of overestimation, that is, the nucleation gap $\pi_0 - \pi_{eq}$, cannot be deduced from our data. We estimated that $\pi_0 = 10$ mN/m for PPP, $\pi_0 = 15$ mN/m for SSS, and $\pi_0 = 20$ mN/m for AAA. From dynamic adsorption isotherms, obtained at a compression rate of 1 cm/min, we find a condensation pressure $\pi_{cond} \approx 8$mN/m for all

three triglycerides. Because π_{eq} must be smaller for AAA than for PPP, we conclude that $\pi_{eq} \leq 10$ mN/m for all three triglycerides. Thus, we arrive at the conclusion that $\pi_{eq} \approx \pi_{cond}$.

For $\pi > \pi_{eq}$, the Langmuir monolayers are thermodynamically unstable at the air—water interface. Under isobaric conditions at $\pi > \pi_0$, slow compression was found for PPP and SSS. The isobaric compression rate is highest for PPP and almost zero for AAA.

LB monolayers can be successfully transferred onto a mica surface. Through the use of the AFM imaging, the thickness of the trident monolayers can be measured. We demonstrated that the apparent thickness depends strongly on the AFM scanning force, and we showed that the compression of the investigated triglycerides is the same. The thickness of the monolayers, obtained by extrapolation to zero-scanning force, is 1.49 for PPP, 1.75 for SSS, and 2.2 nm for AAA. These monolayer thicknesses correspond to tilt angles of the molecules of 46.4, 49.2, and 59.0°, respectively. We conclude that the tilt angle increases when increasing the length of the alkyl chains, that is, the longer chains in the monolayer are more perpendicular to the substrate.

The LB monolayers transferred immediately at surface pressure $\pi > \pi_0$ for PPP and SSS contain domains on top of the monolayer. The molecules in these domains adopt the tuning fork conformation and pack similar as in the crystalline α-and β-crystal phase.

The LB monolayers of PPP and SSS, which were transferred at $\pi \geq \pi_0$, are thermodynamically unstable in air. Small nuclei in tuning fork conformation form on top of the monolayer. For SSS, they are all in β-phase, and for PPP domains with α-like and β-like structures coexist in the LB film. The density of the crystals increases with time. We conclude that the different mobility of the molecules in the trident monolayer of SSS and PPP is the main reason for the different rate of nucleation and growth. For AAA, the monolayer is thermodynamically unstable at the air−mica interface, but the crystallization kinetics are so slow that on the time scale of days they behave as if they were stable.

We conclude that the stability and the kinetics of the Langmuir—Blodgett monolayer depend strongly on the length of the triglycerides alkyl chains and also on the surface pressure at which the deposition takes place. The longer the alkyl chains are, the less mobile the trident monolayer is and the more stable the crystal phase is.The nucleation rate increases with increasing π because the LB monolayer is denser and hence more unstable when the Langmuir layer is transferred at higher π.

References

(1) Charalambous, G.; Doxatakis, G. In *Food Emulsifiers: Chemistry, Technology, Functional Properties, and Applications*; Elsvier: Amsterdam, 1989.
(2) Smith, R.; Berg, J. *J. Colloid Interface Sci.* **1980**, *74*, 273–286.
(3) Fuente, J. F.; Rodriguez Patino, J. M. *Langmuir* **1994**, *10*, 2317–2324.
(4) Fuente, J. F.; Patino, J. M. *Langmuir* **1995**, *11*, 2090–2097.
(5) Sanchez, C. C.; Rodriguez Nino, M.; Rodriguez Patino, J. M. *Colloids Surf., B* **1999**, *12*, 175–192.
(6) Garti, N.; Sato, K. In *Crystallization and Polymorphism of Fats and Fatty Acids*; Marcel Dekker: New York, 1988.
(7) Hamawan, C.; Starov, V. M.; Stapey, A. *Adv. Colloid Interface Sci.* **2006**, *122*, 3–33.
(8) De Jong, S. T. Ph.D. Thesis, University of Utrecht, The Netherlands, 1980.
(9) Bursh, T.; Larsson, K.; Lundquist, M. *Chem. Phys. Lipids* **1968**, *2*, 102–113.
(10) Hamilton, J. A.; Small, D. M. *Proc. Natl. Acad. Sci. U.S.A.* **1981**, *78*, 6878.
(11) Hamilton, J. A. *Biochemistry* **1989**, *28*, 2514–2520.
(12) Claesson, P. M.; Dedinaite, A.; Bergenstahl, B.; Campbell, B.; Christenson, H. *Langmuir* **1997**, *13*, 1682–1688.
(13) Michalski, M.; Brogueira, P.; Goncalves, da Silva, A; Saramago, B. *Eur. J. Lipid Sci. Technol.* **2001**, *103*, 677–682.
(14) Zdravkova, A. N.; Eerden, J. P. J. M *J. Cryst. Growth* **2006**, *293* (2), 528–540.
(15) Hardy, N. J.; Richardson, T. H.; Grunfeld, F. *Colloids Surf., A* **2006**, *284–285*, 202–206.
(16) Akita, C.; Kawaguchi, T.; Kaneko, F.; Yamamuro, O.; Akita, H.; Ono, M.; Suzuki, M. *J. Cryst. Growth* **2005**, *275*, e2187–e2193.
(17) Roberts, G. *Langmuir—Blodgett Films*; Plenum Press: New York, 1990; p 21.
(18) Kjaer, K.; Als-Nielsen, J.; Helm, C.; Tippman-Krayer, P.; Mohwald, J. *J. Phys. Chem.* **1989**, *93*, 3200.
(19) Lin, B.; Shih, M. C.; Bohanon, T. M.; Ice, G. E.; Dutta, P. *Phys. Rev. Lett.* **1990**, *65*, 191.
(20) Schlossman, M.; Schwartz, D.; Pershan, P.; Kawamato, E.; Kellog, J.; Lee, S. *Phys. Rev. Lett.* **1991**, *66*, 1599.
(21) Popovitz-Biro, R.; Wang, J. L.; Majewski, J.; Shavit, E.; Leiserowitz, L.; Lahav, M. *J. Am. Chem. Soc.* **1994**, *116*, 1179.

CG060701T